An *in vitro* study of micromechanics, cellular proliferation and viability on both decellularized porcine dura grafts and native porcine dura grafts

Ashma Sharma[a], **Erika Moore**[b], **Lakiesha N. Williams**[a,*]

[a]J. Crayton Pruitt Family Department of Biomedical Engineering, University of Florida, Gainesville, FL 32611, USA

[b]Fischell Department of Bioengineering, University of Maryland, College Park, MD 20742, USA

Abstract

Damage to the dura mater may occur during intracranial or spinal surgeries, which can result in cerebrospinal fluid leakage and other potentially fatal physiological changes. As a result, biological and synthetic derived scaffolds are typically used to repair dura mater post intracranial or spinal surgeries. The extracellular matrix of xenogeneic dura scaffolds has been shown to exhibit increased cell infiltration and regeneration than synthetic dura materials. In this study, we investigated the biocompatibility of native and decellularized porcine dura by seeding rat fibroblast cells onto the constructs. Cell proliferation, cell viability, and the mechanical properties of these dural grafts were evaluated post-re-seeding on days 3,7 and 14. Live-dead staining and resazurin salts were used to quantify cell viability and cell proliferation, respectively. Micro indentation was conducted to quantify the mechanical integrity of the native and acellular dura graft. The findings indicate that the acellular porcine dura graft creates a beneficial setting for infiltrating rat fibroblast cells. Cell viability, proliferation, and micro indentation results on the acellular grafts are comparable with the native control porcine dura tissue. In conclusion, the porcine scaffold material showed increased cell viability at each time point evaluated. The sustained mechanical response and favorable viability of the cells on the decellularized grafts provide promising insight into the potential use of porcine dura in clinical cranial dura mater graft applications.

*Corresponding author. lwilliams@bme.ufl.edu (L.N. Williams).

Introduction

Cranial dura mater can be damaged during intracranial surgery or traumatic injury resulting in cerebrospinal fluid leakage, infection, or poor wound healing. These issues warrant dura replacement with either a biological or a synthetic graft. The graft material's suitability for the scaffold design is governed by its biocompatibility, mechanical integrity, biodegradability, and scaffold architecture [1,2]. A broad selection of grafts exists; however, no consensus has been reached on an ideal dural substitute. Current gold standards elicit an immune response, lack mechanical integrity upon implantation, and cause complications such as subdural hematomas, brain herniation, and chronic headaches.

Some of the most commonly used commercially available dura scaffold materials are absorbable synthetic material, allografts, and autologous fascia [3–8]. Synthetic materials are convenient as they have an extended shelf life and can be manufactured with customized mechanical properties and increased handleability. However, they do not have a dynamic environment like that of native Extracellular Matrix (ECM) [3]. Synthetics can act as a chronic stimulant on the surrounding tissue, mediating an adverse immune response that clinically manifests as chemical meningitis [9,10]. Additionally, they do not fully mimic the native tissue's mechanical response and have been reported to tear easily during suturing [11]. Autografts and allografts are less prone to infection, but the cost is high, and availability is limited [12–14]. To this end, there is an increased interest in using biological scaffolds derived from xenogeneic tissues due to the complex nature of their ECM, which promotes constructive remodeling [15]. The ECM of biological scaffolds fulfills several crucial functions, including providing structural support to cells, enhancing mechanical properties, delivering bioactive cues, serving as a reservoir for growth factors and their actions, supporting tissue remodeling, and facilitating proper cellular organization [16,17]. Collagen, the primary component of the ECM, contains non-allergenic, non-mutagenic, and non-migratory properties and is a primary reason for interest in using xenogeneic scaffolds [18,19]. The cell-matrix interaction proteins within collagen-based grafts support wound healing and tissue regeneration [20,21]. Incorporating xenogeneic grafts may address the need for biomaterials that mimic the native tissue environment, promote cellular integration, guide tissue regeneration, and ultimately contribute to successful clinical outcomes. Unforeseen immune reactions and infections have been observed after using biological scaffolds such as cadaveric dura or xenograft pericardium [22, 23]. However, there is also evidence that decellularized ECM improves tissue growth and regeneration by allowing fewer complications during repair [16]. Thus, we propose exploring decellularized porcine dura as a cranial dura replacement, which has not been previously considered.

In this study, we evaluate decellularized and native porcine dura mater tissue scaffolds as a replacement for cranial dura through a series of *in vitro* tests, including cell proliferation testing, cell viability testing, and mechanical tests as explained in experimental methods. Here we seed the porcine dura with primary rat fibroblast cells, with our main objectives being to quantify cell viability, cell proliferation, and the mechanical integrity of decellularized porcine dura mater grafts and native porcine dura mater.

Experimental methods

Decellularization

Dura mater was harvested from adult male pigs $n = 6$ (Yorkshire, 6 to 8 months old) at a postmortem time of 2 h at the large animal laboratory at the University of Florida Meat Processing Center (IACUC Protocol #201810442). Porcine dura mater was extracted within 2 h of sacrifice and then washed with phosphate-buffered saline (PBS) solution to remove excess blood and debris. After removing and cleaning, the tissue was cut into circular dura grafts of 14 mm in diameter, followed by decellularization processing using sodium dodecyl sulfate (SDS) solution [2]. The tissues were decellularized for 48 h in the solution and then washed with 1x PBS for 24 h in an orbital shaker. After washing, the tissue was washed with ethanol and sterile saline, alternating three times. The decellularization technique was verified using a DNeasy (QIAGEN®, Germany) kit and a Nanodrop Spectrophotometer (Thermo Fisher Scientific, USA). The decellularized and native tissue were freeze-dried in liquid nitrogen, and the dry weight of tissue samples was measured for DNA content normalization. Nanodrop quantification was done for grafts from $n = 6$ animals for both decellularized and native tissues.

Sterilization and cell seeding

The decellularized dura was further sterilized with peracetic acid (PAA) and ethanol: 2 % PAA/100 % ethanol/dH2O (ratio v/v/v = 2/1/1) for 2–4 h, followed by multiple washes in sterile PBS to remove residual acid. The sterility was evaluated by incubating the dura sample in a cell culture medium (10 % fetal bovine serum)(ThermoFisher, USA), 1 % antibiotic antimycotic (ThermoFisher, USA), and Dulbecco's modified eagle medium (ThermoFisher, USA) in 5 % CO_2 at 37 °C. The medium was dispensed in the empty wells as a control. Samples were assessed daily, and color changes were taken to indicate contamination.

Once the sterility was confirmed, decellularized 14 mm diameter tissue grafts were placed in the same 24-well plate used for cell seeding. The graft tissue was placed in the cell medium for 24 h before seeding. After 24 h, they were removed from the medium and kept in the biological safety cabinet for approximately 1 hour to dry the excess medium for better cell attachment. Sprague Dawley rat lung fibroblast cells were isolated and used to seed all grafts. In the cell seeding process, the mixture containing 2×10^6 rat lung fibroblast cells and 100 μL cell culture medium was added in a dropwise manner to the decellularized porcine dura graft to avoid attachment to the plastic surface. Furthermore, 1 mL of additional cell culture medium was added to the seeded dura grafts after one hour of the initial seeding process to ensure cell attachment. In the current study, all testing and analyses were conducted at three specific time points: 3 days, 7 days, and 14 days after initial seeding, and the cell culture media was changed daily.

Histological analysis

Freshly isolated native, decellularized, and re-seeded dura mater of randomly assigned male pigs were fixed using formalin for all time points, embedded in paraffin, and sectioned at 4 μm thickness. Next, the sectioned tissue was stained with hematoxylin & eosin (H&E)

to confirm collagen fiber integrity, cell number density, and area fraction of collagen fibers. The area fraction of collagen fibers within the native and decellularized dura mater ($n = 3$ per native and $n = 3$ per decellularized) was analyzed with ImageJ software (National Institutes of Health) [24].

Cell viability

Cell viability at the three-time points was determined by calcein AM and ethidium-homodimer (ThermoFisher, USA). Cell-seeded constructs were incubated in serum-free media supplemented with 4 mmol/l calceinAM and 2 mmol/l ethidium-homodimer for one hour at 37°C. Constructs were then washed with PBS and covered with glass coverslips. Next, the constructs were immediately scanned using a fluorescence microscope (Leica DFC 300 FX, Leica Microsystems, Wetzlar, Germany). The live cells were analyzed, using Image J, and quantified as the number of green stained cells.

Cell proliferation

The cell proliferation assay was performed at three time points (3, 7, and 14 days) using resazurin stock solution with a concentration of 5 mM. The resazurin stock solution was prepared by dissolving resazurin powder (resazurin sodium salt) into distilled water. Furthermore, the resazurin working solution was prepared by mixing 10 % of the resazurin stock solution with the cell culture medium. The re-seeded dura graft samples for the three-time points were then incubated in a resazurin working solution for 4 h at 37 °C with a 5 % CO_2 atmosphere to convert resazurin to resorufin. Reduction percentage refers to the degree of reduction of the Alamar blue by proliferating cells. The higher percentage of reduction means the greater proliferation of cells in culture.

Triplicate aliquots of 100 mL of the incubated resazurin working solution were taken to measure fluorescent intensity using a microplate reader (SpectraMax M5/M5e) at a wavelength of 590 nm. Metabolic activity of the cells, given by the percent reduction of the assay (PRA), was measured using Eqn. (i), where plain resazurin working solution was taken as the untreated control, the autoclaved solution was taken as 100 % reduced, and the absorbance values were calculated [25,26].

$$PRA = \frac{(\text{Fl 590 sample} - \text{Fl 590 of untreated control})}{(\text{Fl 590 of autoclaved} - \text{Fl590 of untreated control})} * 100$$

(i)

Micro indentation

The fresh samples were indented using a custom-built piezo-electric stage (P-628.1 CD, Physik Instrumente) along with a piezo amplifier (E-625.CR Servo Controller, Physik Instrumente) [27]. A custom-made spherical indenter (dia. of 8 micrometers) was used to indent the sample at five locations. Four samples were indented at each time point for the native ($n = 4$ male pigs per time point) and decellularized tissue ($n = 4$ male pigs). All tests were performed at room temperature, and PBS was sprayed for hydration. The thickness of the sample was measured at three different locations using a vernier caliper (accuracy of 0.01 mm) and averaged. All tests were conducted at room temperature, following a

trapezoidal loading-holding-unloading pattern. For instrument calibration, the noise profile was checked and kept less than the threshold value (approximately 10μN). If the threshold was higher, the system was recalibrated two times to avoid the noise. Minimum force was set at 0 μN and the load displacement was set at 10 % of the sample height. The loading and unloading process involved a total indentation depth of 100 μm at a rate of 10 μm/s, with a 60-second holding time between the loading and unloading stages. The indentation force gradually increased during loading, followed by a decrease in response to the holding period. Subsequently, the force gradually decreased during unloading [27,28]. Towards the end of unloading, the force turned negative due to tissue adhesion, but it returned to its initial value once the indenter separated from the sample [29–31]. LabVIEW software was utilized to analyze the indentation data. The Hertz contact model was used to determine the elastic modulus (E_{Hert})using force as a function of indentation depth [28,32].

$$F(t) = \frac{4E_{Hertz}(\sqrt{R})\delta(t)^{\frac{3}{2}}}{3\left(1 - v^2\right)}$$

(ii)

where F = force calibrated by stiffness and displacement, R is the radius of the tip, δ is the indentation depth, and v is the Poisson's ratio.

The Hertz contact model was then rearranged to determine the effective modulus as a function of time for soft samples in quasi-static conditions.

$$E_{effective}(t) = \frac{3(Ft)\left(1 - v^2\right)}{4(\sqrt{R})\delta(t)^{\frac{3}{2}}}$$

(iii)

where R = 4 μm, δ is 100 μm, and v is 0.5 [33].

The effective modulus at the equilibrium steady state modulus (SSM) is similar to the stress relaxation modulus when $t = \infty$ [34].

Equation (iii) was fitted to the relaxation phase of our indentation results using the MATLAB curve fit tool to calculate the steady-state modulus [27,32,35]. Further, the Goodness of Fit function in MATLAB was used to evaluate fits using NMSE whose values were above 0.8 [36].

Statistical analysis

All experimental results were expressed as mean ± standard deviation. The Shapiro-wilk test was conducted to examine normality and the results showed that the data was not significantly different with p-value>0.1. A one-way ANOVA followed by a posthoc test for multiple pairwise comparisons was performed to evaluate statistical differences between the native, decellularized, and re-seeded dura mater at three time points. A value of $p < 0.05$ is assumed to be statistically significant in this study.

Results

Decellularization

A slight thickness reduction was observed in the decellularized dura. The average thickness of native dura mater is 0.69 ± 0.20 mm and 0.65 ± 0.15 mm for decellularized dura mater. The thicknesses are not significantly different. The DNA content of decellularized dura mater is less than 50 ng per mg dry weight. As shown via spectrophotometry, the DNA content is 423.33 ± 69.58 ng/mg and 32.75 ± 8.84 ng/mg for native and decellularized samples, respectively. An unpaired T-test for DNA content reflected significant differences in native and decellularized samples with a p-value of 0.009 ($p < 0.05$).

Histology

The histological images show the lateral view of dura mater after 3, 7, and 14 days of re-seeding in native and decellularized conditions (Fig. 1). The Hematoxylin and Eosin (H & E) stained images show the dura mater's fiber morphology (pink). As shown in a previous publication, our decellularization process efficiently removed all cells from the ECM of dura [2]. Therefore, as expected, the fibroblasts (blue dots indicated by red arrows) were absent in the decellularized tissues, while they were observed in both the seeded and native dura. These results indicate that the procedure used for decellularizing and re-seeding in the current study was adequate.

The area fraction of dura mater, which is taken as the ratio of the area of fibers to the total area, was calculated to determine the effect of decellularization and re-seeding on the structure of dura mater. The area fraction of collagen represented by the histogram, as shown in Fig. 2, was calculated to be 0.897 ± 0.046 for native tissue, 0.902 ± 0.059 for decellularized tissue, 0.864 ± 0.030 at 3 days, 0.902 ± 0.028 at 7 days, and 0.916 ± 0.001 at 14 days post-re-seeding. The P-value determined from the one-way ANOVA conducted on the obtained data in each sample condition was greater than 0.05, indicating statistically insignificant results.

Fig. 3 shows a consistent increase in cell count for native and re-seeded dura mater at three different time points. Based on the Image J analysis, the number of cells (H & E stained nuclei) was calculated as 90 ± 6, 182 ± 22, and 280 ± 18 for the dura mater after 3, 7, and 14 days of re-seeding, respectively, and 492 ± 9 cells in native condition. As intended, the cell count increased with the increasing number of days after the re-seeding process, while the native dura mater still had the highest number of cells. Furthermore, from the one-way ANOVA along with the post hoc test, the p-value was determined to be less than 0.05 for all conditions, indicating that the cell count data obtained for dura mater at different days after re-seeding were statistically different (Table 1).

Cell viability

Cell viability testing using live dead staining was performed to analyze the health and growth of cells in dura mater tissues after 3, 7, and 14 days of re-seeding. These results were compared with the one observed for native dura mater in Fig. 4. Green illuminated features shown in Fig. 4 represent the live cells, while the red features represent dead cells. In all the

images shown in Fig. 4, the presence of red (dead) cells was not evident, and the cell number and cell proliferation were observed to increase as the time point advanced in the case of re-seeded samples.

Cell proliferation

Percentage Reduction Assay (PRA) values were calculated using Eqn. (i) for re-seeded dura mater at the three different time points (3, 7, and 14 days) to determine the metabolic activity of fibroblast cells. Fig. 5 shows the PRA values to be lower on days 3 and 7 than on day 14, which may be associated with higher metabolic activity. The percentage reduction in the test well increased as the time points increased, indicating cell metabolic activity. Like all other analyses, one-way ANOVA and post-hoc tests were performed for the PRA values at different time points. The PRA values obtained for 3 and 7 days were not statistically different (*P*-value of 0.3). On the other hand, results obtained for 3 and 14 days (*P*-value of 0.0002) and 7 and 14 (*P*-value of 0.002) after re-seeding were statistically different.

Micro indentation

The steady-state modulus was calculated for native, decellularized, and re-seeded samples for 3,7 and 14 days. The indentation force increased gradually during loading, decreased in response to holding, and decreased gradually during unloading. Towards the end of unloading, the force became negative in response to tissue adhesion and returned to its initial value upon indenter-sample separation [28]. Results show that the steady state modulus slightly increased in decellularized dura compared to the native dura. The average steady-state moduli of native dura is 2127.75 ± 15.20 Pa, 2725 ± 237 Pa for the decellularized dura, 2025.7 ± 168.18 Pa for the tissue 3 days after re-seeding, 2455.15 ± 495 Pa for tissue 7 days after re-seeding, and 2259.46 ± 284.51 Pa for tissue 14 days after re-seeding (Fig. 6). The comparison of native, decellularized tissue and tissue post re-seeding using one-way ANOVA followed by post hoc test did not show significant differences in micro indentation (*p*-value greater than 0.2) (Table 2).

Discussion

The number of cells within the re-seeded dura graft proliferated with the increase in the number of days. The highest number of cells was seen in the sample after 14 days of re-seeding, while the lowest cell count was seen in the sample after 3 days of re-seeding (Figs. 1 and 3). In contrast, the change in the area fraction of collagen (Fig. 2) was observed to be statistically insignificant within decellularized, native, and re-seeded tissue, which implies that the re-seeding process did not change the amount of collagen in the microstructure of dura mater. Studies have shown that the chemical decellularization methods usually lead to certain destruction in fibers [37], and the chemical detergent with sodium dodecyl sulfate may compromise the fiber substrate [38,39]. However, the DNA content within the dura tissue after decellularization decreased by more than 90 % and is less than 50 ng per mg dry weight, which is adequate to satisfy the intent of decellularization [40]. Cell proliferation may also indicate that the decellularization process provides a suitable ECM, facilitating cell attachment and promoting tissue regeneration [41].

Fibroblasts in the ECM are very important in understanding cellular activity, remodeling, and proliferation tendencies. It is important to note that cell count analysis estimates the number of cells in the sample but does not indicate viability. The cell viability results presented in Fig. 4 showed that a small number of scattered live cells were present at the superficial layer of the tissue after three days of the re-seeding process, while after seven days, the number of live cells increased. After 14 days of re-seeding, the cells were observed to be more elongated in shape and highly interconnected with the surface, akin to that of a fibroblast cell. The random and interconnected pattern of cells also indicated that the cells were infiltrated in the extracellular matrix up to 14 days post re-seeding. A similar pattern where cells were stable with good graft integration was also reported in a study by Elson et al. [42].

Metabolic activities such as cell viability, cytocompatibility of biomaterials, and cell proliferation were quantitively evaluated. Cytocompatibility testing using the resazurin-based assay was used because of its high sensitivity and cost-effectiveness. Resazurin, a cell-permeable and virtually nonfluorescent dye, is reduced to resorufin due to cellular metabolism (i.e., DNA content and glucose consumption), which changes its color. Based on the color change, the PRA was determined using Eqn. (i), which provided a quantitative measure of proliferation [26]. The percentage of reduction increased from day 3 to day 14, which is consistent with the number of cells being greater at 14 days after re-seeding compared to 3 days and 7 days. However, the cell growth rate slowed after 7 days. Slow growth may result from the coverage of free area available on the scaffold and the lack of new surface area to grow, as also indicated by Dan et al. [43]. The study by Ng et al. revealed a lack of linear correlation of reduction assay with high cell density, which supports the slower growth rate in this study after 7 days [44]. In this study, after 7 days, the cells could have gone into arrest after reaching a certain degree of confluency which might have caused apoptosis and, thus a slow increase in the percentage of reduction [45].

Micro-indentation testing showed that the steady-state compressive modulus of the decellularized dura was similar to the native dura (native dura: 2127 ± 15 Pa, decellularized dura:2725 ± 237 Pa). Also, the one-way ANOVA reveals that the steady state modulus for three days, seven days, and fourteen days post re-seeding were similar with a P-value greater than 0.05(3 days: 2025 ± 168 Pa, 7 days: 2455 ± 495 Pa, and 14 days: 2259 ± 284 Pa). The compressive modulus calculated from micro indentation revealed that the mechanics of the native tissue was preserved after decellularization. Additionally, the mechanics were similar post re-seeding. The compressive modulus calculated from micro indentation is challenging to compare across soft tissue because the response depends on the indentation depth and loading rate [27]. We specifically controlled those in our experimental protocol. In soft matter, when the indentation rate increases, it takes less time to dissipate energy, eventually increasing the stiffness [32]. When the thickness is inconsistent, the indentation rate changes the moduli [29–31]. Loading in the compressive stress state locally under micro indentation is likely the reason for the resulting different moduli values from uniaxial global compression tests. Although the location was controlled, thickness variations and the number of cells across the dura mater may have caused some of the scatterings of the steady-state compressive modulus.

An adequate cranial dural substitute should have various long-term and short-term characteristics. These include appropriate strength, a thickness similar to that of native tissue, minimal inflammation, minimal scarring, and minimal risk of transmission of infectious diseases [6, 46]. Our *in vitro* evaluation of the scaffold is a standard method for direct comparison across the material. The regenerative process is very complex, and in this *in vitro* study, we do not attempt to mimic the condition for clinical applications. Nevertheless, our study successfully captures the features for tissue regeneration to lend insight into *in vivo* applications using decellularized porcine dura mater.

Limitations of the study

Despite stringent location control, thickness variations and variances in the number of cells across the dura mater might have resulted in some scattering of the steady-state compressive modulus. Thus, capturing thickness across the graft through a visual method would be ideal. An *in vivo* study is essential to replicate the clinical conditions accurately for potential clinical applications. One of the limitations in micro indentation is the presence of noise within the 10–20 % range of Fmax, alongside the limited resolution of the indenter in relation to the measured values.

Conclusions

In conclusion, this study revealed that a xenogeneic scaffold derived from decellularized porcine dura has a similar architecture as native porcine dura. The microstructural analysis of collagen fibers confirms that the structural integrity of the graft remains intact over the prescribed time points. Here, a stable scaffold supported cell attachment and proliferation over 14 days. Future work will include *in vivo* subcutaneous testing using an animal model. This data will allow for assessing the feasibility of using the current porcine dura model as a future replacement for native dura in the clinic.

Supplementary Material

Refer to Web version on PubMed Central for supplementary material.

Acknowledgments

Data availability

No data was used for the research described in the article.

References

[1]. Chan BP, Leong KW, Scaffolding in tissue engineering: general approaches and tissue-specific considerations, Eur. Spine (2008), 10.1007/s00586-008-0745-3.

[2]. Sharma A, Liao J, Williams LN, Structure and mechanics of native and decellularized porcine cranial dura mater, Eng. Regener 4 (2023) 205–213, 10.1016/j.engreg.2023.02.004.

[3]. O'Brien FJ, Biomaterials & scaffolds for tissue engineering, Mater. Today 14 (3) (2011) 88–95, 10.1016/S1369-7021(11)70058-X.

[4]. Reddy MSB, Ponnamma D, Choudhary R, Sadasivuni KK, A comparative review of natural and synthetic biopolymer composite scaffolds, Polymers 13 (7) (2021), 10.3390/polym13071105 (Basel).

[5]. Deng K, et al. , Evaluation of efficacy and biocompatibility of a new absorbable synthetic substitute as a dural onlay graft in a large animal model, Neurol. Res. (2016), 10.1080/01616412.2016.1214418.

[6]. Marchand E, Anson JA, Bovine pericardium for dural grafts: clinical results in 35 patients, Neurosurgery 39 (4) (1996) 764–768, 10.1097/00006123-199610000-00025. [PubMed: 8880771]

[7]. Martínez-Lage JF, Pérez-Espejo MA, Palazón JH, Hernández FL, Puerta P, Autologous tissues for dural grafting in children: a report of 56 cases, Child Nervous Syst 22 (2) (2005) 139–144, 10.1007/S00381-005-1232-3.

[8]. Bejjani GK, Zabramski J, Safety and efficacy of the porcine small intestinal submucosa dural substitute: results of a prospective multicenter study and literature review, J. Neurosurg. 106 (6) (2007) 1028–1033, 10.3171/JNS.2007.106.6.1028. [PubMed: 17564175]

[9]. Kitano M, et al. , Subdural patch graft technique for watertight closure of large dural defects in extended transsphenoidal surgery, Neurosurgery 54 (3) (2004) 653–661, 10.1227/01.NEU.0000108780.72365.DC. [PubMed: 15028140]

[10]. Kelly DF, Oskouian RJ, Fineman I, Collagen sponge repair of small cerebrospinal fluid leaks obviates tissue grafts and cerebrospinal fluid diversion after pituitary surgery, Neurosurgery 49 (4) (2001) 885–890, 10.1097/00006123-200110000-00020. [PubMed: 11564250]

[11]. Macewan MR, Kovacs T, Osbun J, and Ray WZ, Comparative analysis of a fully-synthetic nanofabricated dura substitute and bovine collagen dura substitute in a large animal model of dural repair, 2018, doi: 10.1016/j.inat.2018.05.001.

[12]. Abuzayed B, Kafadar AM, Oğuzoğlu A, Canbaz B, Kaynar MY, Duraplasty using autologous fascia lata reinforced by on-site pedicled muscle flap: technical note, J. Craniofac. Surg. 20 (2) (2009) 435–438, 10.1097/SCS.0B013E31819B968F. [PubMed: 19326487]

[13]. Nishioka H, Izawa H, Ikeda Y, Namatame H, Fukami S, Haraoka J, Dural suturing for repair of cerebrospinal fluid leak in transnasal transsphenoidal surgery, Acta Neurochir. 151 (11) (2009) 1427–1430, 10.1007/S00701-009-0406-2 (Wien). [PubMed: 19499173]

[14]. Angelos PC, Downs BW, Options for the management of forehead and scalp defects, Facial Plast. Surg. Clin. N. Am 17 (3) (2009) 379–393, 10.1016/J.FSC.2009.05.001.

[15]. Pittenger MF, et al., Multilineage Potential of Adult Human Mesenchymal Stem Cells, 284, Academic Press, 1999, pp. 143–147, 10.1126/science.284.5411.143.

[16]. Faulk DM, Johnson SA, Badylak SF, Decellularized biological scaffolds for cardiac repair and regeneration, Cardiac Regener. Repair Biomater. Tissue Eng. (2014) 180–200, 10.1533/9780857096715.2.180.

[17]. Achinger KG, Williams LN, Trends in CSF leakage associated with duraplasty in infratentorial procedures over the last 20 years: a systematic review, Crit. Review 51 (2) (2023) 33–44, 10.1615/CRITREVBIOMEDENG.V51.I2.30, trade; in Biomedical Engineering.

[18]. Garcia Y, Collighan R, Griffin M, Pandit A, Assessment of cell viability in a three-dimensional enzymatically cross-linked collagen scaffold, J. Mater. Sci. Mater. Med. (2007), 10.1007/s10856-007-3091-9.

[19]. Lee CH, Singla A, and Lee Y, "Biomedical applications of collagen," 2001. [Online]. Available: www.elsevier.com/locate/ijpharm.

[20]. Ferreira AM, Gentile P, Chiono V, Ciardelli G, Collagen for bone tissue regeneration, Acta Biomater. 8 (9) (2012) 3191–3200, 10.1016/J.ACTBIO.2012.06.014. [PubMed: 22705634]

[21]. Rothamel D, Schwarz F, Sculean A, Herten M, Scherbaum W, Becker J, Biocompatibility of various collagen membranes in cultures of human PDL fibroblasts and human osteoblast-like cells, Clin. Oral Implants Res 15 (4) (2004) 443–449, 10.1111/J.1600-0501.2004.01039.X. [PubMed: 15248879]

[22]. Salyer KE, Bruce DA, Hardin CE, Hopkins KS, Gendler E, Craniofacial neurosurgical approach for extensive hyperostotic meningioma, J. Craniofac. Surg. 4 (3) (1993) 128–133, 10.1097/00001665-199307000-00004. [PubMed: 8241354]

[23]. Velnar T, Gradisnik L, Soft tissue grafts for dural reconstruction after meningioma surgery, Bosn. J. Basic Med. Sci 19 (3) (2019) 297, 10.17305/BJBMS.2019.3949. [PubMed: 30877836]

[24]. Clemons TD, et al. , Coherency image analysis to quantify collagen architecture: implications in scar assessment, RSC Adv. 8 (18) (2018) 9661–9669, 10.1039/C7RA12693J. [PubMed: 35540841]

[25]. Uzarski JS, DiVito MD, Wertheim JA, Miller WM, Essential design considerations for the resazurin reduction assay to noninvasively quantify cell expansion within perfused extracellular matrix scaffolds, Biomaterials 129 (2017), 10.1016/j.biomaterials.2017.02.015.

[26]. Kumar P, Nagarajan A, Uchil PD, Analysis of cell viability by the alamarBlue assay, Cold Spring Harb. Protoc. 2018 (6) (2018), 10.1101/PDB.PROT095489 p. pdb.prot095489.

[27]. Rubiano A, Galitz C, Simmons CS, Mechanical characterization by mesoscale indentation: advantages and pitfalls for tissue and scaffolds, Tissue Eng. Part C Methods (2019), 10.1089/ten.tec.2018.0372.

[28]. Weickenmeier J, de Rooij R, Budday S, Ovaert TC, Kuhl E, The mechanical importance of myelination in the central nervous system, J. Mech. Behav. Biomed. Mater (2017), 10.1016/j.jmbbm.2017.04.017.

[29]. MacManus DB, Pierrat B, Murphy JG, Gilchrist MD, Protection of cortex by overlying meninges tissue during dynamic indentation of the adolescent brain, Acta Biomater. 57 (2017) 384–394, 10.1016/J.ACTBIO.2017.05.022. [PubMed: 28501711]

[30]. Menichetti A, MacManus DB, Gilchrist MD, Depreitere B, Vander Sloten J, Famaey N, Regional characterization of the dynamic mechanical properties of human brain tissue by microindentation, Int. J. Eng. Sci 155 (2020), 103355, 10.1016/J.IJENGSCI.2020.103355.

[31]. Walsh DR, Zhou Z, Li X, Kearns J, Newport DT, and Mulvihill JJE, "Mechanical properties of the cranial meninges: a systematic review," https://home.liebertpub.com/neu, vol. 38, no. 13, pp. 1748–1761, Jun 2021, doi: 10.1089/NEU.2020.7288.

[32]. Budday S, et al. , Mechanical properties of gray and white matter brain tissue by indentation, J. Mech. Behav. Biomed. Mater (2015), 10.1016/j.jmbbm.2015.02.024.

[33]. Persson C, Evans S, Marsh R, Summers JL, Hall RM, Poisson's ratio and strain rate dependency of the constitutive behavior of spinal dura mater, Ann. Biomed. Eng. 38 (3) (2010) 975–983, 10.1007/S10439-010-9924-6. [PubMed: 20087767]

[34]. Bush BG, Shapiro JM, DelRio FW, Cook RF, Oyen ML, Mechanical measurements of heterogeneity and length scale effects in PEG-based hydrogels, Soft Matter (2015), 10.1039/c5sm01210d.

[35]. Cowin SC and Doty SB, Tissue mechanics. 2007. doi: 10.1007/978-0-387-49985-7.

[36]. MacManus DB, Pierrat B, Murphy JG, Gilchrist MD, Dynamic mechanical properties of murine brain tissue using micro-indentation, J. Biomech. 48 (12) (2015) 3213–3218, 10.1016/J.JBIOMECH.2015.06.028. [PubMed: 26189093]

[37]. Luo X, et al. , *In vitro* evaluation of decellularized ECM-derived surgical scaffold biomaterials, J. Biomed. Mater. Res. B Appl. Biomater 105 (3) (2017) 585–593, 10.1002/JBM.B.33572. [PubMed: 26663848]

[38]. Asarias JR, Nguyen PT, Mings JR, Gehrich AP, Pierce LM, Influence of mesh materials on the expression of mediators involved in wound healing, J Invest Surg 24 (2) (2011) 87–98, 10.3109/08941939.2010.548904. [PubMed: 21345009]

[39]. Morrison WA, Hussey AJ, Extracellular matrix as a bioactive material for soft tissue reconstruction, ANZ J. Surg. 76 (12) (2006) 1047, 10.1111/J.1445-2197.2006.03970.X. [PubMed: 17199686]

[40]. Crapo PM, Gilbert TW, Badylak SF, An overview of tissue and whole organ decellularization processes, Biomaterials 32 (12) (2011) 3233–3243, 10.1016/j.biomaterials.2011.01.057. [PubMed: 21296410]

[41]. Zwirner J, Ondruschka B, Scholze M, Schulze-Tanzil G, Hammer N, Mechanical and morphological description of human acellular dura mater as a scaffold for surgical reconstruction, J. Mech. Behav. Biomed. Mater. (2019), 10.1016/j.jmbbm.2019.04.035.

[42]. Elson KM, et al. , Non-destructive monitoring of viability in an ex vivo organ culture model of osteochondral tissue, Eur. Cell Mater. 29 (2015), 10.22203/eCM.v029a27.

[43]. Dan Y, et al. , Development of novel biocomposite scaffold of chitosan-gelatin/ nanohydroxyapatite for potential bone tissue engineering applications, Nanoscale Res. Lett 11 (1) (2016) 1–6, 10.1186/S11671-016-1669-1. [PubMed: 26729219]

[44]. Ng KW, Leong DTW, Hutmacher DW, The challenge to measure cell proliferation in two and three dimensions, Tissue Eng. 11 (1–2) (2005) 182–191, 10.1089/TEN.2005.11.182. [PubMed: 15738673]

[45]. Camasão DB, et al. , Increasing cell seeding density improves elastin expression and mechanical properties in collagen gel-based scaffolds cellularized with smooth muscle cells, Biotechnol. J (2019), 10.1002/biot.201700768.

[46]. Li Q, Zhang F, Wang H, Pan T, Preparation and characterization of a novel acellular swim bladder as dura mater substitute, Neurol. Res. 41 (3) (2019) 242–249, 10.1080/01616412.2018.1550139. [PubMed: 30912483]
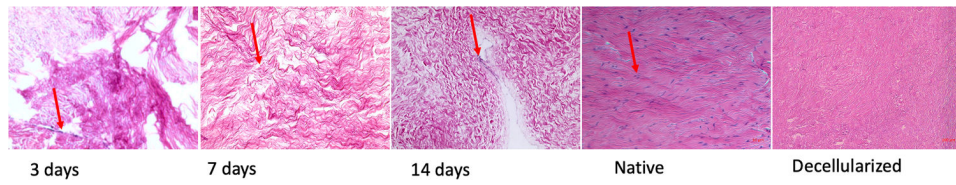
Fig. 1.
H &E stained images of dura mater in the transverse direction at 20X magnification (scale Bar 100 μm) at 3, 7, and 14 days after re-seeding compared with decellularized and native tissue (red arrow represents the presence of cells).
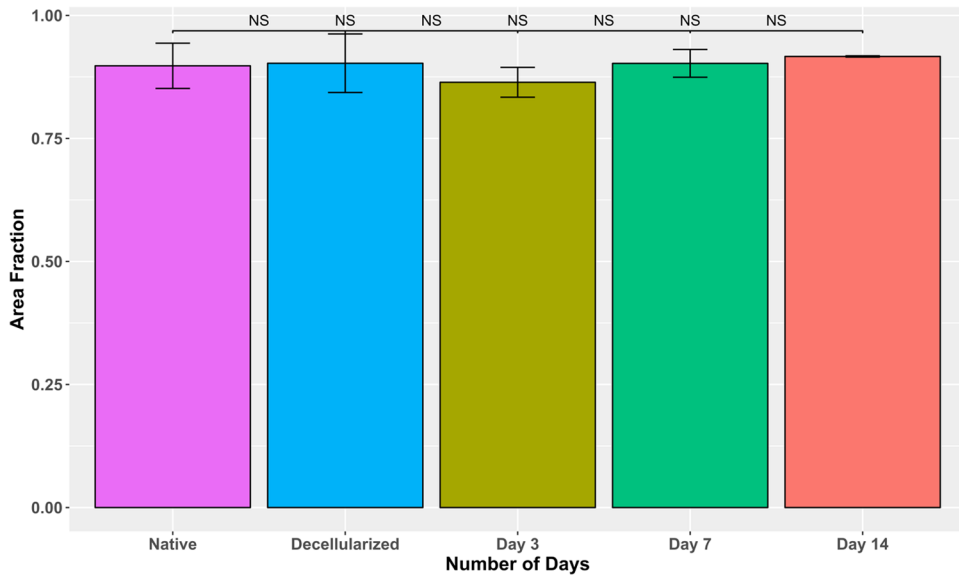
Fig. 2.
The area fraction of collagen fibers of native dura, decellularized dura pre-seeding, and re-seeded dura tissue at prescribed time points (3 days, 7 days, and 14 days) (no significant differences between groups ('NS' represents no significant differences).
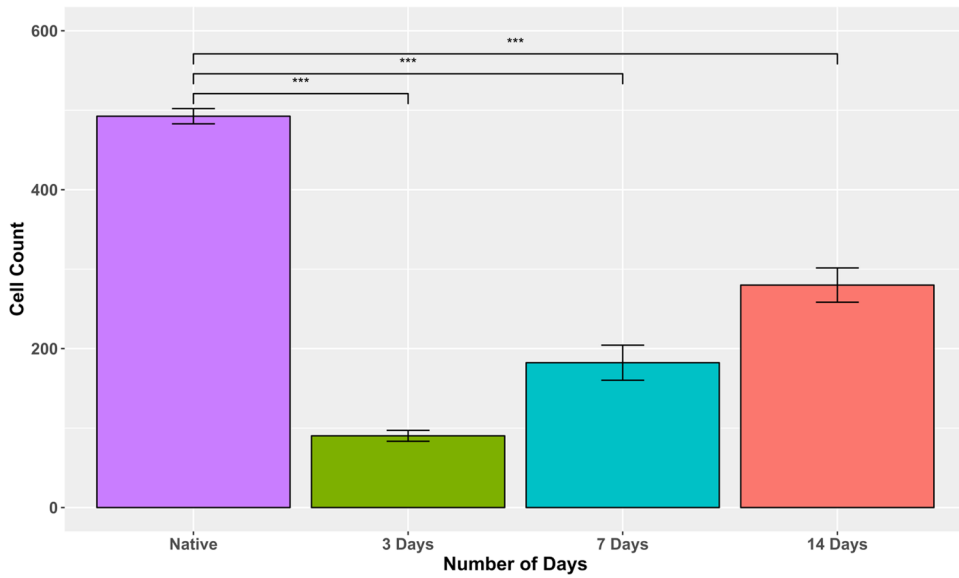
Fig. 3.
Bar graph of cell count of re-seeded dura mater at 3 days, 7 days, and 14 days post re-seeding compared with native tissue (Location for cell count: four corners and two central areas)('***' represent significant difference $P < 0.001$).
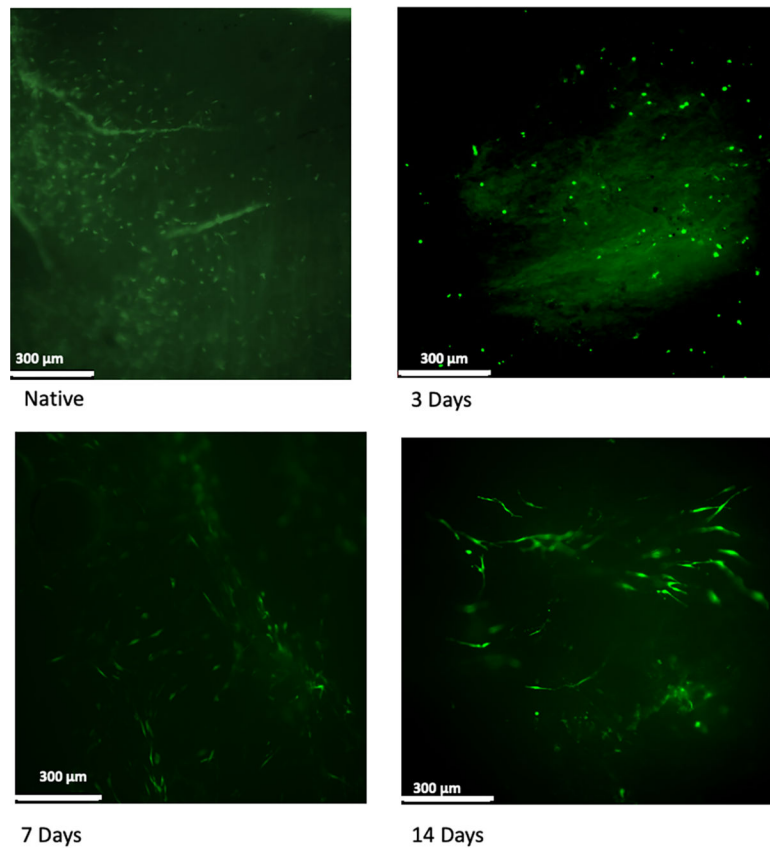
Fig. 4.
Live dead staining image of the fibroblast cells grown on the prepared sample after 3 days,7 days, and 14 days of incubation compared with native dura matter. Live cells are shown in green (scale Bar 300 μm).
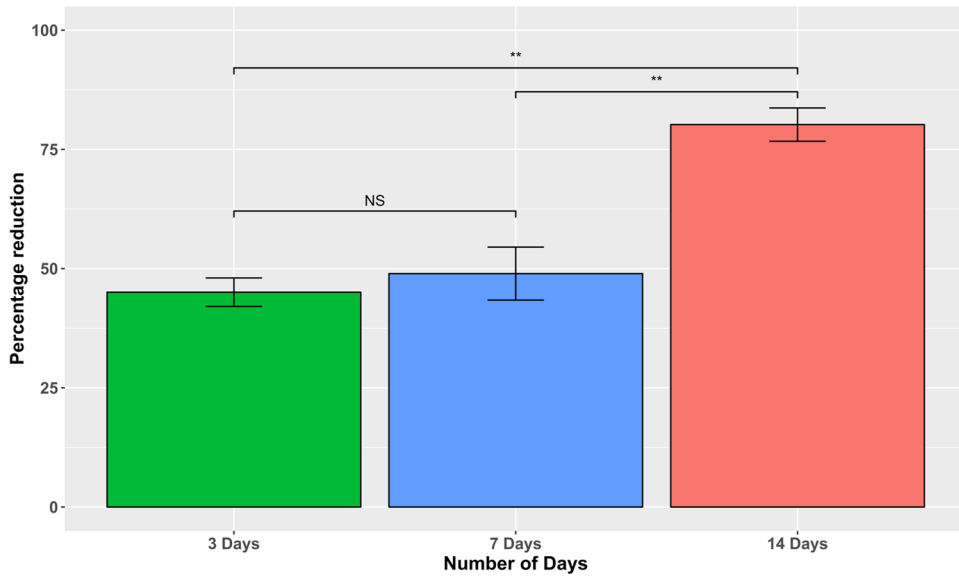
Fig. 5.
Proliferation of fibroblast cells on the prepared sample using percentage reduction of resazurin assay using fluorescence ('NS' represent no significant differences, while '**', represent significant differences($P < 0.01$).
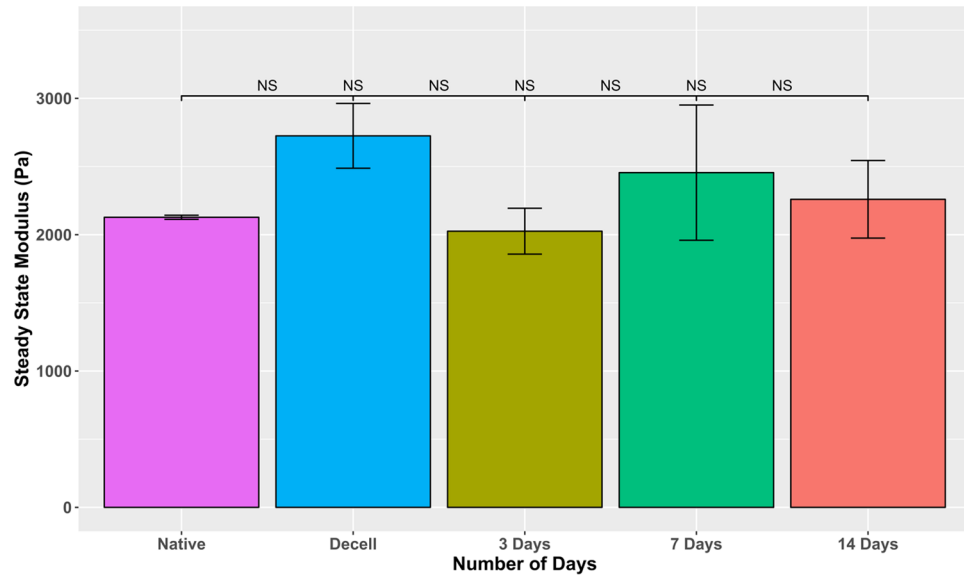
Fig. 6.
Bar Graph of effective modulus from micro indentation at 3, 7, and 14 days after re-seeding on native and decellularized dura ('NS' on all bar graphs represents no significant differences).

Table 1

P-value determined by post hoc test for all conditions of cell count data obtained for dura mater on different days after re-seeding.

	Native	**Day 3**	**Day 7**	**Day 14**
Native	-	0.	0	0
Day 3	0	-	0.0000229	0
Day 7	0	0.0000229	-	0.0000123
Day 14	0	0	0.0000123	-

Table 2

P-values determined by post hoc test for proliferation using resazurin assay for dura mater at different days after re-seeding.

	3 days	7 days	14 days
3 days	-	0.625	0.00142
7 days	0.625	-	0.0018
14 days	0.00142	0.0023	-